Russian Journal of Earth Sciences, Vol. 23, ES2004
https://doi.org/10.2205/2023ES000835
© Authors 2023.
CC BY

Tectonic Activities Description in the Ongoing Collision Zone of the Eurasia-Arabia Plates Using 2D Surface Waves Tomography

Seyed Hossein Abrehdari*[,1,2], Jon K. Karapetyan[1], Habib Rahimi[2], and Eduard Geodakyan[1]

[1] *Institute of Geophysics and Engineering Seismology, National Academy of Sciences, Gyumri, Republic of Armenia*
[2] *Institute of Geophysics, University of Tehran, Tehran, Iran*

Received 11 September 2022; accepted 14 November 2022; published 11 May 2023.

In order to better understand the regional tectonic activities of the continent-continent ongoing collision-compressed edge zone of the Eurasian-Arabic plates, 2D tomography maps of the Caucasus territory using the Rayleigh waves were generated. The 2D tomography images of this study, illustrate the large variety in surface wave propagation velocity in different complex geologic units of the Caucasus. To draw the 2D tomography maps, we accomplished a 2D-linear inversion procedure on the Rayleigh wave dispersion curves for the periods of 5 to 70 s (depth ≃ 180 km). To conduct this, local-regional data from ~ 1300 earthquakes ($M \geq 3.9$) recorded by the 49 broadband stations from 1999 to 2018 in a wide area with complicated tectonic units were used. In comparison with results of previous studies in Caucasus, the tomography maps for the long-periods (T = 50–70 s; depth ~ 180 km) are more influenced by the velocity structure of the uppermost mantle which demonstrate the ultralow and ultrahigh-velocity anomalies. The results for the medium-periods ($30 \leq T \leq 45$ s), the low-velocity zones coincide with areas thought to be correlated with underplating of the lower crust (e.g., shallow LAB), while, the high-velocity zones are usually demonstrating the presence of a normal continental crust over a stable and thick or oceanic-like lid. Short-periods ($5 \leq T \leq 25$ s) are more influenced by the ever-evolving deformations of the geological units, sedimentary basins, volcanic complexes, uplifts, and reveals a low-velocity small zone, on the NW slope of the Aragats volcano (depth ≃ 7 km), which is different from the results of other studies.

Keywords: The Caucasus territory, Tectonic activities, 2D surface wave tomography, Group velocity maps, 2D linear inversion

Citation: Abrehdari, S. H., J. K. Karapetyan, H. Rahimi, and E. Geodakyan (2023), Tectonic Activities Description in the Ongoing Collision Zone of the Eurasia-Arabia Plates Using 2D Surface Waves Tomography, *Russian Journal of Earth Sciences*, Vol. 23, ES2004, doi: 10.2205/2023ES000835.

1 Introduction

The Caucasus Collision Zone consists of an assemblage of lithospheric blocks, which have a complex tectonic setting that is created by the collision and convergence of the Arabian plate towards Eurasia resulting from the Iranian part of the Alpine-Himalayan collision (Figure 1).

The Caucasus is a region between the Caspian Sea and the Black Sea, which is divided into two parts, the South Caucasus (Lesser Caucasus) and the North Caucasus (Greater Caucasus). Greater and Lesser Caucasus are separated by the Transcaucasian (Dzirula) Massif, Kura and Rioni rivers in the middle. The Caucasus includes Armenia, Georgia, Azerbaijan, NW Iran, East of Turkey, and parts of Russia country. The convergence between Arabia and Eurasia began in Late Cretaceous [*Golonka*, 2004]. Over time, this motion led to subsequent collision stages between Arabia and smaller continental blocks resulted from the break-up of Gondwana until the final closure of Neotethys Ocean.

Correspondence to:
*Seyed Hossein Abrehdari, abrehdari@ut.ac.ir

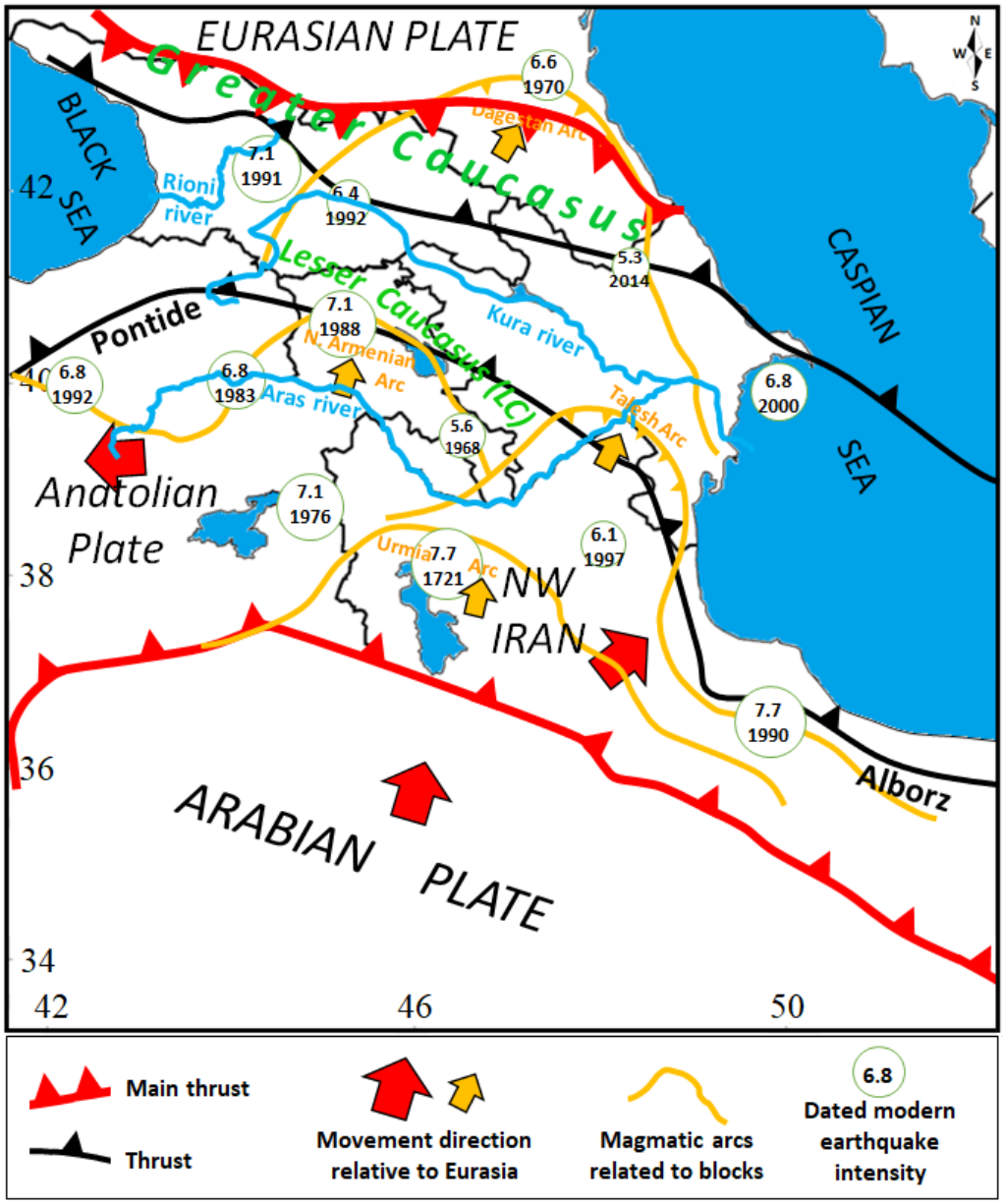

Figure 1: The Caucasus active tectonic features. Retrieved from [*Jrbashyan et al.*, 2001; *Khuduzade and Jafarov*, 2017].

The structures from the so called Caucasian collision are specified by compressional structures, including thrusts, nappes, reverse faults and strongly related deformed fault-propagation folds. In contrast to these faults, the transversal faults are also mainly compressional structures having a more or less considerable strike-slip component. According to some studies [e.g., *Sun et al.*, 2012] this continent-continent collisional tectonics processes begun about 12 Ma. The Caucasus region is compressed between Arabian-Eurasian plates and due to NNW 338° at a rate of 28 mm/year [*DeMets et al.*, 1990], compression expanded the main seismo-active structures in NW Iran, Greater Caucasus (GC), Lesser Caucasus (LC), Eastern Anatolian Accretionary Complex (EAAC).

The fault zones include the reverse strike-slip, strike-slip sinistral, strike-slip dextral, wrench, and major thrust faults with WNW–ESE direction are developed; and also the extensional axes with N–S direction relative movement of the Arabian plate against the Eurasian plate are formed.

The Greater Caucasus ranges consist mostly of Paleozoic metasedimentary rocks and granitoids, Jurassic sediments, Mesozoic and Cenozoic volcanism [*Sosson et al.*, 2017]. According to some studies [e.g., *Ismail-Zadeh et al.*, 2020] the Lesser Caucasus ranges consist of Paleozoic granitoid metamorphic basement overlain unconformably by shelf carbonates of Paleozoic Triassic age. They also contain ophiolite mélange lithologies of the Sevan-Akera and the Vedi suture zones. The base-

ment rocks and the ophiolites are overlain by the extensive volcano-sedimentary sequence of Late Eocene-Early Miocene age. In this enigmatic area, there are complicated geological structures and large volcanic complexes and basins (e.g., South Caspian Basin (SCB), Rioni Basin (RB), Kura Basin (KB), Eastern Black Sea Basin (EBSB), Sevan Depressions, Central Armenia Block (CAB), Elbrus, Aragats, Ararat, Kazbek).

The ultimate goal of this study is to generate two-dimensional tomography images using Rayleigh wave dispersion characteristics for investigating the upper mantle up to the crust of the Caucasus area. In this domain many studies have been done to image the tomography velocity maps using different tomography methods, and most of the studies have been conducted by body waves on a large-small-scale and deep.

Since the amplitudes of surface waves are many times greater than those of body waves and they conceal the body waves in seismic records and make it difficult to process and interpret; and also because seismic surface waves sample the near surface of the Earth rather than deep Earth, they are especially suitable to use in surveys for environmental or Geotechnical applications. The best way of using seismic surface waves in extracting information on the subsurface is to compute their dispersion relationships and then to apply an inversion scheme to the obtained dispersion curves [*Jin and Colby*, 1991]. Therefore, preparing 2D tomographic maps and accurate imaging of the geological structure based on surface wave dispersion curves is useful for investigating the velocity structure of the study area and we chose this method.

We applied 2D inversion procedure to generate tomography images of the Caucasus for understanding the velocity structure of the features of the structure of the lithosphere based on increasing and decreasing wave velocity anomalies. The Rayleigh wave group velocity dispersion curves for each source-station path (single-station method) using the Herrmann's `do_mft` package [*Herrmann*, 2013] was estimated. Then, using a 2D-linear inversion method developed by Ditmar and Yanovskaya [*Ditmar and Yanovskaya*, 1987] and Yanovskaya and Ditmar [*Yanovskaya and Ditmar*, 1990], the 2D group velocity maps were generated. To do this, the local-regional earthquake data recorded by the 49 broadband stations (Table 1) were used. The results of tomography maps are presented for a period of 5 to 70 s. Our results for the lower periods show distinct velocity anomalies in the basins, along the faults, and beneath the volcanoes. The velocity maps for the medium and the long periods reveal fast and ultra slow velocity anomalies in the different geological units of the Caucasus.

Some tomography studies have been conducted related to the estimation of the crustal thickness beneath this region e.g., NW Iran: [*Rahimi et al.*, 2014], EAAC: [*Skobeltsyn et al.*, 2014], Caucasus: [*Koulakov et al.*, 2012; *Zabelina et al.*, 2016]. Our results are consistent with structures of the major geological units in the region and outcomes of the mentioned studies as well. However, the existence of a denser network of stations could be helpful in determining small-scale or large-scale velocity anomalies. This study benefits from a rich earthquake database (1999–2018) and new permanent seismic stations installed in NW Iran, Russia, Armenia, Turkey, Azerbaijan, and Georgia, which provides much better ray path coverage in the Caucasus for the resolution of tomography velocity images. In interpreting the tomographic maps of this study, the results of other studies of various tomographic methods performed in the Caucasus to provide more comprehensive information to researchers were used.

2 Data and resolution parameters of the tomography images

2.1 Data

The study area is situated in the territory of the Caucasus with Longitude: 38°–53° and Latitude: 37°–44° Figure 2a, b. Figure 2a–2f shows the study area, epicenters of earthquakes, stations, paths coverage and histogram of ray distribution with respect to the periods. To conducte this study about 19 years (~1300 local-regional events; $M \geq 3.9$ and 30,000 vertical (Z) component) seismic data, collected during 1999–2018 recorded by Seismic Network Incorporated Research Institutions for Seismology (IRIS), Iranian Seismological Center (IRSC), International Institute of Earthquake Engineering and Seismology (IIEES), and temporary network of the Institute for Advanced Studies in Basic Sciences (IASBS) were processed. Seismic network consists of 49 broadband seismometers.

2.2 Images resolution parameters

The resolution and density of the paths and their balance distribution in our case study depend on the geometry of the seismic array and earthquakes data distribution that can limit the number of available paths for some directions. The dense raypath controls the validity-high resolution of tomography maps (red shads in Figure 3 and 6 – averaging area (L) and stretching ε). So, the number of paths change for different periods and depth (see section Appendix A, Table A1 and Figure 6). Figure 6 show the variations in resolution parameters such as the stretching (ε), averaging

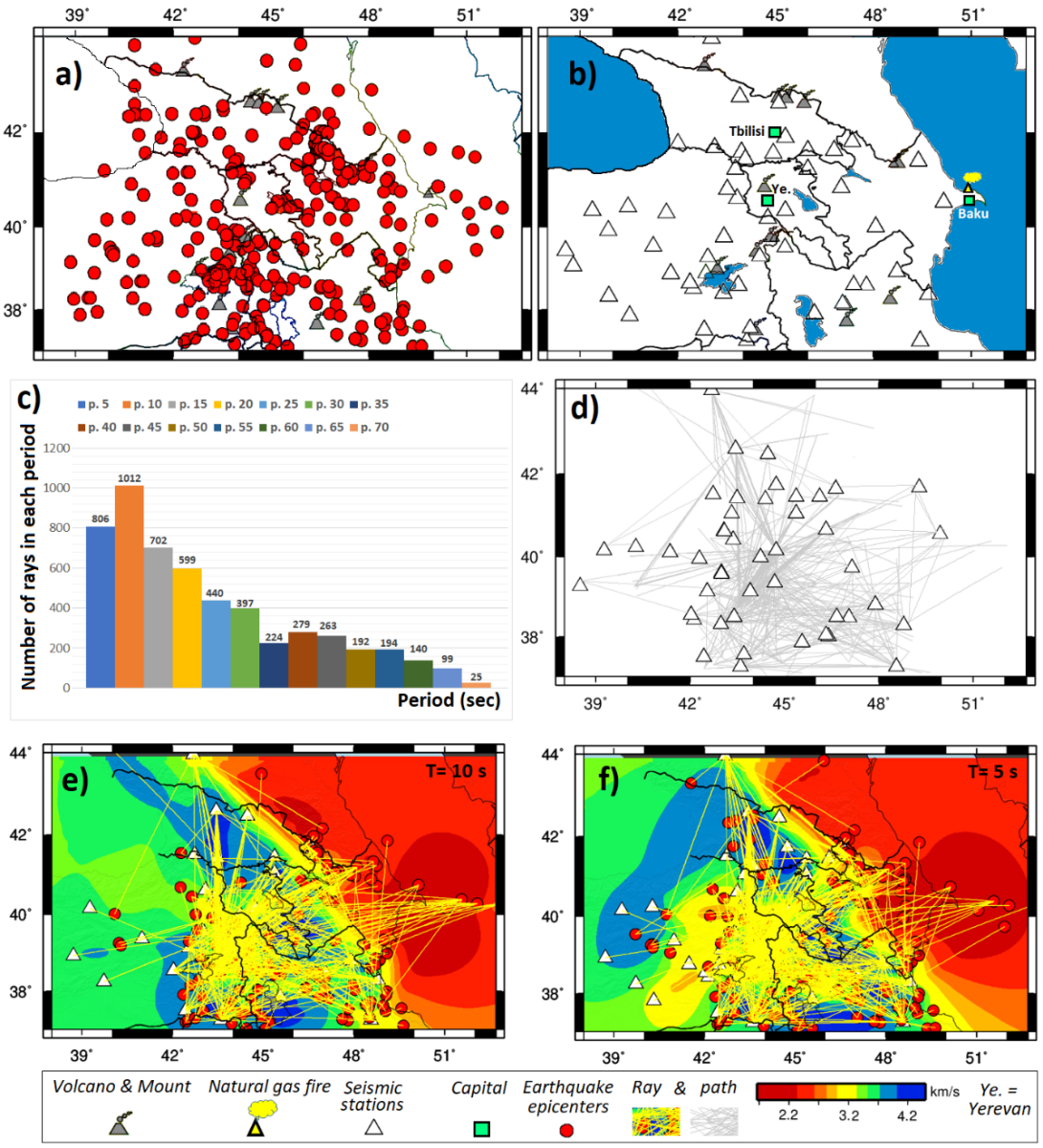

Figure 2: The earthquakes (red circles) used in this study. b) Locations of the stations. c) The number of rays in each period comparative to the period in this study. d) Distribution of stations and inter-station path coverage at period 40 s. Figures e–d, f show the ray paths coverage (yellow lines) at period 5 and 10 s.

area (L), data density, velocity, and cell size of the $0.2° \times 0.5°$ (20×50 km^2) for the periods of short-medium-long in this study.

The Yanovskaya's methodology [*Yanovskaya*, 1997] to calculate the spatial resolution and the azimuthal coverage was used, which varies from 20 to 50 km in the study region. A functional $S(x,y)$ is calculated for different orientations of the coordinate system in order to determine sizes of the averaging area along different directions.

The averaging area, can be approximated by an ellipse, centred at a point of the study region, with axes equal to the largest and the smallest values of $S(x,y)$. The size of the averaging area along different directions are defined by $S(x,y)$, which gives an idea of the resolution in each point (x,y). It is approximated by an ellipse with half-axes of the $S_{\max}(x,y)$ and $S_{\min}(x,y)$. The smallest $[S_{\min}(x,y)]$ and largest $[S_{\max}(x,y)]$ axes of the ellipse are calculated, and the resolution at each point is given by the mean size of the averaging area:

$$L = (S_{\min}(x,y) + S_{\max}(x,y))/2.$$

The resolution length in a tomographic inversion is approximated with an ellipse at the centre of a point, which gives us an estimate of the resolution [*Yanovskaya et al.*, 1998]. The resolution length defines the mean size of the averaging area (L)

Table 1: Information of the considered seismic networks in study area

Station Code	Station name	Longitude (◦)	Latitude (◦)	Network Code	Data Center Website
GNI / GSS	Garni, Armenia	44.7241	40.1341	IU (IRIS/USGS)	A0: National Seismic Network of Armenia https://www.fdsn.org/networks/?initial=G
GANJ	Ganja, Azerbaijan	46.3297	40.6519	IU (IRIS/USGS)	AB: National Seismic Network of Azerbaijan https://www.fdsn.org/networks/detail/AB/
QZX	Qazah, Azerbaijan	45.3721	41.0481	IU (IRIS/USGS)	
ZKT	Zakatala, Azerbaijan	46.6311	41.6411	IU (IRIS/USGS)	
GOB	Qobu, Azerbaijan	49.7130	40.4047	RSSCA	Republican Seismic Survey Center of Azerbaijan https://www.seismology.az/
AKH	Akhalkalaki	43.4929	41.4111	IU (IRIS/USGS)	GO: National Seismic Network of Georgia https://www.fdsn.org/networks/detail/GO/
BATM	—	41.6936	41.6041	IU (IRIS/USGS)	
BGD	Ninotsminda	43.5985	41.2645	IU (IRIS/USGS)	
CHVG	Chkavaleri	42.0841	42.71833	IU (IRIS/USGS)	
DDFL	Dedoflistskaro	46.1183	41.44580	IU (IRIS/USGS)	
DGRG	DGRG - GAREJI	45.3731	41.45072	IU (IRIS/USGS)	
GUDG	Gudauri	44.4772	42.4646	IU (IRIS/USGS)	
KZRT	Kazreti	44.3987	41.3866	IU (IRIS/USGS)	
LGD	Lagodekhi	46.2421	41.8343	IU (IRIS/USGS)	
ONI	Oni	43.4524	42.5905	IU (IRIS/USGS)	
SEAG	TbilisiSea	44.8036	41.7635	IU (IRIS/USGS)	
TBLG	Delisi, Georgia	44.7381	41.7309	IU (IRIS/USGS)	
TRLG	Trialeti	44.1017	41.5392	IU (IRIS/USGS)	
ANDN	ANDIRIN, TURKEY	37.5811	36.3452	IU (IRIS/USGS)	TU: National Seismic Network of Turkey (DDA) https://www.fdsn.org/networks/detail/TU/
AYDN	TASOLUK, TURKEY	37.6608	27.8792	IU (IRIS/USGS)	
BALY	BALYA, TURKEY	39.7403	27.6195	IU (IRIS/USGS)	
BORA	ESKISEHIR, TURKEY	39.8801	30.4534	IU (IRIS/USGS)	
DIGO	KARS, TURKEY	40.4147	43.3742	IU (IRIS/USGS)	
EPOS	POSOF, TURKEY	41.5035	42.7279	IU (IRIS/USGS)	
ERBA	ERBA, TURKEY	40.6814	36.7547	IU (IRIS/USGS)	
HAKT	HAKKARI, TURKEY	37.5579	43.7071	IU (IRIS/USGS)	
ILGA	ILGAZ, TURKEY	41.0521	33.7165	IU (IRIS/USGS)	
KELT	KELKIT, TURKEY	40.1486	39.2556	IU (IRIS/USGS)	
KEMA	KEMALIYE, TURKEY	39.2688	38.4932	IU (IRIS/USGS)	
VANB	Gevas, Van sir	39.57798	28.63232	IU (IRIS/USGS)	TK: National Strong-Motion Network of Turkey (TR-NSMN) https://www.fdsn.org/networks/detail/TK/
CUKT	Gerede, Bolu	40.7924	32.2059	IU (IRIS/USGS)	
TASB	Tefenni, Burdur	37.3160	29.7791	IU (IRIS/USGS)	
MLAZ	Merkez, Edirne	41.6704	26.5858	IU (IRIS/USGS)	
AKDM	Merkez, Erzurum	39.8733	41.2226	IU (IRIS/USGS)	
AGRB	Iskenderun, Hatay	36.5571	36.1747	IU (IRIS/USGS)	
SIRT	Karaburun, Izmir	38.6390	26.5127	IU (IRIS/USGS)	
GURO	Marmaris, Mugla	36.8394	28.2448	IU (IRIS/USGS)	
KARS	Susehri, Sivas	40.1692	38.1063	IU (IRIS/USGS)	
DIGO	Dursunbey, Balike	38.2963	43.1197	IU (IRIS/USGS)	
FTBB	—	46.3944	38.0171	IRSC	Iranian Seismological Center (IRSC) http://www.irsc.ut.ac.ir/istn.php
TAHR	—	47.0513	38.4894	IRSC	
TBZ	Tabriz	46.1498	38.2348	IRSC	
TVRZ	—	46.6675	38.5042	IRSC	
BRND	—	48.5680	37.2483	IASBS	Institute for Advanced Studies in Basic Sciences (IASBS), https://iasbs.ac.ir
KUTE	—	48.8038	38.3046	IASBS	
SARA	Sarab	45.5654	37.8634	IASBS	
GRMI	Germi (Ardebil)	47.8940	38.8100	INSN	Iranian National Seismological Center http://www.iiees.ac.ir/
MAKU	Maku (Urmia)	44.6829	39.3550	INSN	(http://www.iiees.ac.ir/en/iranian-national-broadband-seismic-network/)
KIV	Kislovodsk, Russia	43.9562	42.6888	IRISDMC	II: Global Seismograph Network - IRIS/IDA https://www.fdsn.org/networks/detail/II/

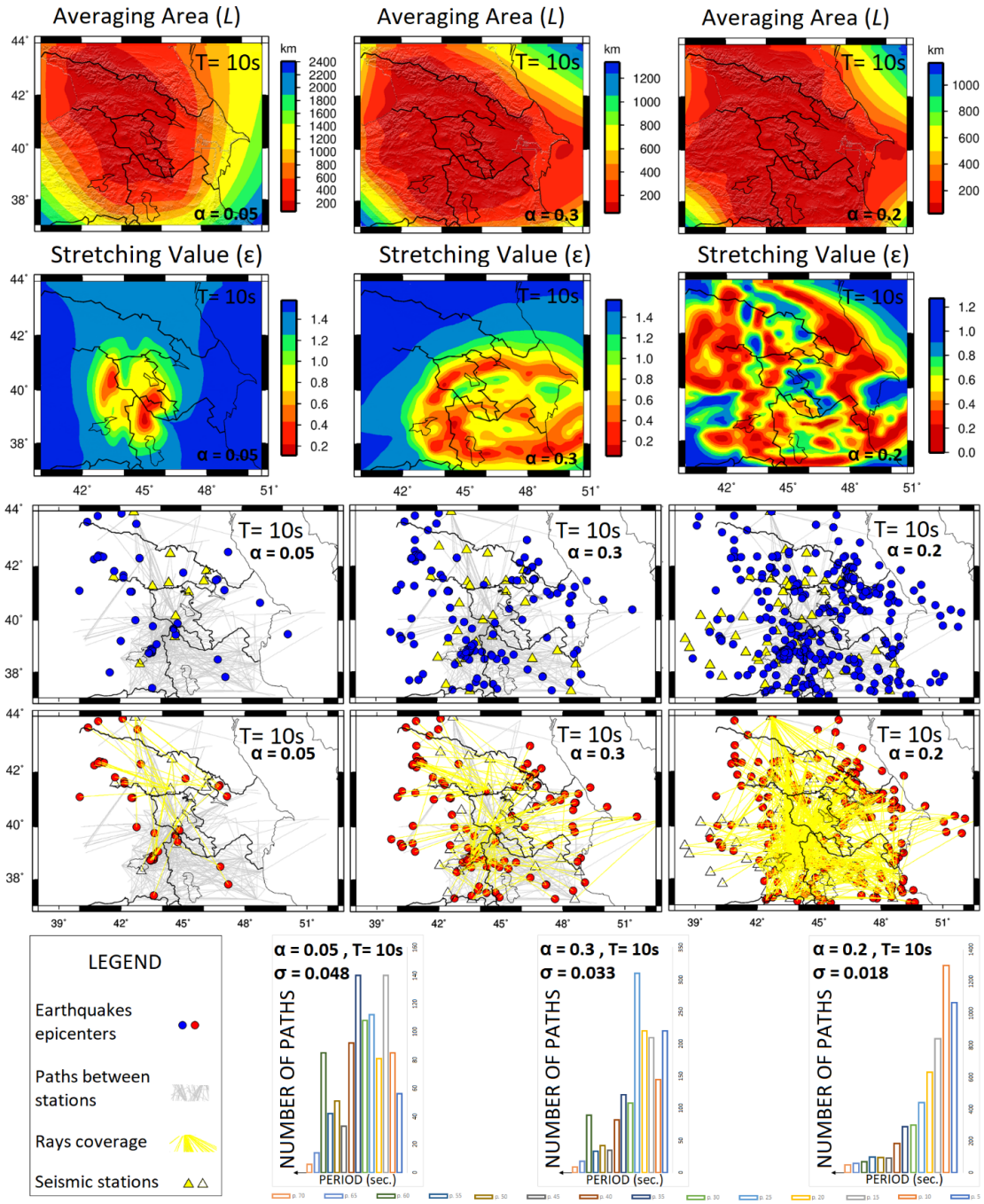

Figure 3: The important role of the regularization parameter (α) in tomography images resolution. Calculations of group velocity maps are imaged for several regularization parameter (α). Decrease in α gives a sharper solution region with an increase in solution error, whereas increasing α results in smoothing of the solution region with decreasing solution error. The small solution errors by testing different α values ($\alpha = 0.1$, 0.2, and 0.3) and observing the number of rays path passing through each cell size of $0.2° \times 0.5°$ by running the specialized computer codes in MATLAB software, which was determined in this study. The σ is an estimate of the standard error of the data.

for tomography maps by just using Figure 3 and 6 estimates, as the overall resolution which has a much uniform structure due to increased number of paths.

The second test for the quality of the tomographic inversion is the stretching (ε) parameter of the averaging area which defines how ray paths are uniformly distributed which provides information on the azimuthual distribution of the ray paths and is given by the ratio:

$$\varepsilon = (S_{\max}(x,y) - S_{\min}(x,y)) / (S_{\max}(x,y) + S_{\min}(x,y)).$$

Large values of the stretching (ε) parameter (usually $\varepsilon > 1$) imply that the paths have a preferred orientation and along this preferential direction is likely to be quite small. On the contrary, small values of the stretching (ε) parameter imply that the paths are more or less uniformly distributed along all directions; hence the resolution at each point can be represented by the mean size of the averaging area (Figure 3 and 6, Table A1).

Figure 3 shows the important role of the regularization parameter (α) in 2D tomography images resolution (e.g., number of paths in each period, distribution of stations and earthquakes, ray coverage between seismic epicenters-stations). Distribution of stations and earthquakes determines the amount the data density, which is beyond our control. The values of the stretching (ε) are between 0.5 and 0.95 in most part of the study area at the fourteen periods. The averaging area value is larger than ~150, with its maximum equal to ~2800. This indicates that the azimuthal distribution of the paths is sufficiently uniform and the resolution is almost the same along any direction. The dense rays path distribution (Figure 3 and 6, $\alpha = 0.2$) controls the reliability and the high resolution of tomography results (red shads in averaging area (L) and stretching (ε)).

Therefore, stretching (ε) and averaging area (L) values are two parameters that indicate the orientation and resolution of the different areas within the study area for each period and at any latitude (Y) and longitude (X) direction. Figure 6 illustrates the variation of all parameters for periods of 5–70 s. The Yanovskaya's methodology is used to calculate the spatial resolution, which varies from 20 to 50 km in our study region. We constructed the high resolution 2D tomography velocity model in Caucasus by inverting the pure path of Rayleigh wave dispersion curves at 1050 ($35 \times 30 = 1050$) nodes using a grid with cell size of $0.2° \times 0.5°$ (20×50 km^2) (Figure 6). As mentioned, the data density shows the distribution of stations and earthquakes, which is beyond our control.

3 Methodology

3.1 Dispersion curves measurement

The first step for the calculation of surface waves dispersion curves is the exploratory analysis of the waveform data to select the events with acceptable signal-to-noise ratios (SNR). The Rayleigh dispersion curves have been extracted from the vertical (Z) components of the velocity records, after removing the instrument responses given by the calibration sheet of the instruments.

After preparing the earthquakes waveform and preliminary corrections on it, for each station-earthquake pair (single-station method), the group velocity dispersion curve of Rayleigh waves by applying the Herrmann's `do_mft` package [*Herrmann*, 2013] to the vertical (Z) component of motion on each event is estimated. Modified `sacmft96` work around problems with improper station and component specifications in Sac files. `Sacmft96` is called `do_mft` for interactive analysis of group velocities and spectral amplitudes. SAC (Seismic Analysis Code) is a general purpose interactive program designed for the study of sequential signals, especially time series data.

In fact, the frequency-time analysis of surface waves is used to estimate the dispersion curves. This method is used for estimating phase and group velocity of surface waves. It passed the preprocessed signal through a system of narrow-band filters in which the central frequency is varying and the amplitude of filter outputs is visualized in time and frequency domains. Then, on the `do_mft` diagram, the group velocity dispersion curve for each path is obtained. Figure 4 shows an example of determining group velocity dispersion curve for the vertical (Z) component of the Garni (GNI) station (Armenia) using `do_mft` processing.

To conduct this, we applied Herrmann's `do_mft` package on waveforms of ~1300 earthquakes recorded by the 49 stations in the Caucasus region. We then processed more than ~30,000 vertical (Z) component of dispersion curves (Figure 4g). For this purpose, first, in Ubuntu system the earthquake data (miniSEED format) was converted to a SAC file format and then the fundamental mode of the Rayleigh wave for each vertical (Z) component using the `do_mft` package was determined.

3.2 Group velocity measurement and data quality

The number of inter-station paths increases with the square of the number of stations, but not all paths can be used to obtain a high-quality dispersion curve. The number of inter-station paths increases with the square of the number of stations, but not all paths can be used to obtain a high-quality dispersion curve. In order to obtain a valid tomography output and minimize the workload, some data quality control criteria should be considered to identify and remove incorrect measurements.

In this study, we use three criteria to select data: First, selecting the events with minimum $M \geq 3.9$ and reject $M \leq 3.8$ due few dispersion points that can be picked and the large variations. Second, the SNR greater than 5 (to analysis and make a good data bank in time domain, which it is not affected much for different period ranges of 5 to 70 s in our study). The range and signal-to-noise ratio (SNR) of the data between 10 seconds

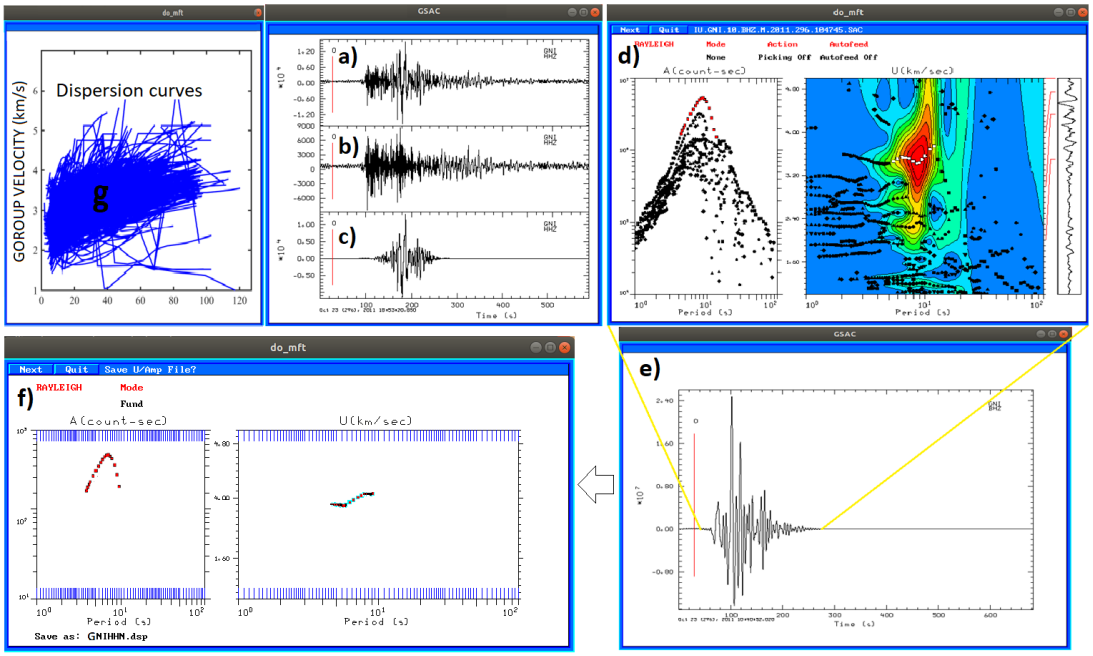

Figure 4: Different steps of determining the dispersion curve (fundamental mode- red shade) using `do_mft` package. a) Raw waveform, b) radial component, c) cleaned seismogram traces recorded in GNI (Garni, Armenia) station. d) high-energy area of the seismic signal to determine the dispersion curve using `do_mft` package and its energy peak e) cleaned seismogram traces f) the picked dispersion curve related high-energy area (the spectral amplitude of fundamental mode) of the seismic signal in d, and g) dispersion curves ($\sim 30,000$ curves). The vertical red lines (with the alphabet 'O' above them) show the onset of chosen pickfile by SAC software (automatic default of start reading of arrival time).

and 100 seconds is desirable, and in this research, the data with low S/N have been omitted. In fact, we measure the group velocity of the dispersive Rayleigh wave by using multichannel Fourier transformation (MFT) method [e.g., *Herrmann and Ammon*, 2004] between 5–70 s (Figure 4g).

The third criterion on the quality of the solution is travel time residual (unaccounted) (σ). Since it has been assumed that the unaccounted residuals are random, σ can be accepted as an estimate of the standard error of the data. As soon as a solution for lateral velocity variations is obtained, remaining travel time residuals are calculated along all paths. Some of them may be large due to measurement errors and other factors. To decrease the effect of large errors, the data with the residuals larger than 3σ are rejected, and the procedure of tomographic reconstruction is repeated. Such selection of the data is performed several times, until no large residuals are remained in the data set [*Yanovskaya et al.*, 1998]. The standard deviation (σ) with selecting the regularization parameter $\alpha = 0.2$ is reasonably low which showing the stability of the method (Figure 6).

3.3 Inversion and 2D tomography

We applied the inversion technique developed by Ditmar-Yanovskaya [*Ditmar and Yanovskaya*, 1987] to generate the local group velocity maps at selected periods 5 to 70 s. The result of this tomography technique is the distribution of group velocities at different grid points throughout the region, which are used to generate group velocity maps. For each period, the tomographic method finds the solutions of group velocities, $V(x,y)$, that minimize the following function:

$$(d - Gm)^T (d - GM) + \alpha \iint |\nabla_m(X)|^2 dX = \min$$

in which $d = t - t_0$ is an input data vector, and t_0 are observed and computed travel time along each path, G is data kernel, and $m(x,y)$ is defined as:

$$m(X) = (V^{-1}(X) - V_0^{-1})V_0,$$

where x and y indicate the longitude and latitude, respectively, $V(x,y)$ is the group velocity at point (x,y), V_0 is the reference average group velocity, and α is a parameter that controls the trade-off of smoothness and fitness of the output velocities. Increasing α parameter means increasing the smoothness and reducing the fitness and conversely.

Phase velocity maps are calculated by testing several regularization parameters ($\alpha = 0.05$, 0.1, 0.2 and 0.3). Decrease in α gives a sharper solution region with an increase in solution error, whereas

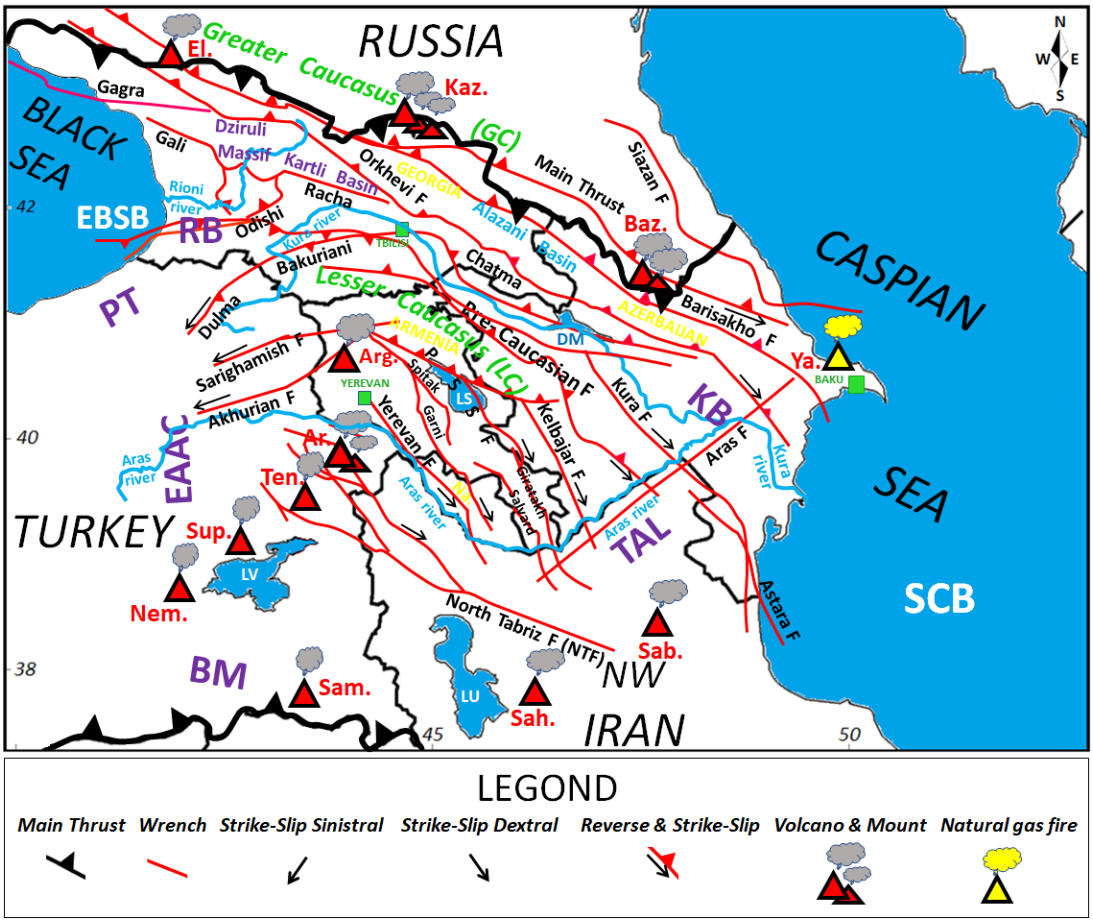

Figure 5: The Central Eurasian-Arabian collision zone and labeled geological units discussed in the interpretation of 2D tomography maps of the study area. Retrieved from [*Adamia et al.*, 2011]. Abbreviations: F = fault, Sab. = Sabalan, Sah. = Sahand, Sam. = Samadi, Nem. = Nemrout, Sup. = Suphan, Ten. = Tendourek, Ar. = Ararat, EAAC = East Anatolian Accretionary Complex, Arg. = Aragats, El. = Elbrus, Kaz. = Kazbek, Ya. = Yanardag (natural gas fire on a hillside), RB = Rioni Basin, PT = Pontide, BM = Bitlis Massif, TAL = Talesh, KB = Kura Basin, LV = Lake Van, LU = Lake Urmia, LS = Lake Sevan, MD = Mingachevir Dam, SCB = South Caspian Basin, EBSB = Eastern Blake Sea Basin, Na. = Nakhchivan, and PSSF = Pambak-Sevan-Syunik Fault. The thick black line denotes major plate boundaries in Caucasus.

increase in α leads to a smoothing of the solution region with decrease in solution error. We used the value of $\alpha = 0.2$, which gives relatively smooth maps with small solution errors. *The small solution errors by testing different α values and observing the number of rays passing through each cell size of $0.2° \times 0.5°$ by running the specialized computer codes in MATLAB software in this study was conducted (see Figure 3). So, did not use the old methods (such as the checkerboard test).*

4 Interpretation of the results of tomographic maps for different periods

Figure 5 shows the labeled geological units (e.g., GC, LC, SCB, ...), faults, volcanoes, rivers, and basins that used for interpretation the 2D tomography maps in this study.

Since the velocity of waves in the Earth increases with increasing depth, the longer wavelength (low frequency) waves can travel faster than the shorter wavelength (high frequency) waves. The propagation velocity of seismic waves depends on density and elasticity of the medium as well as the type of wave. Velocity tends to increase with depth through Earth's crust and mantle, but drops sharply going from the mantle to outer core. Typical speeds for Rayleigh waves are on the order of 1 to 5 km/s [*Ammon*, 2019].

The earthquakes waves are originating in Earth's crust or upper mantle, which travel more rapidly through cold, dense regions, and more slowly through hotter rocks. In accordance with the commentary of seismic tomography images [e.g., *Be-*

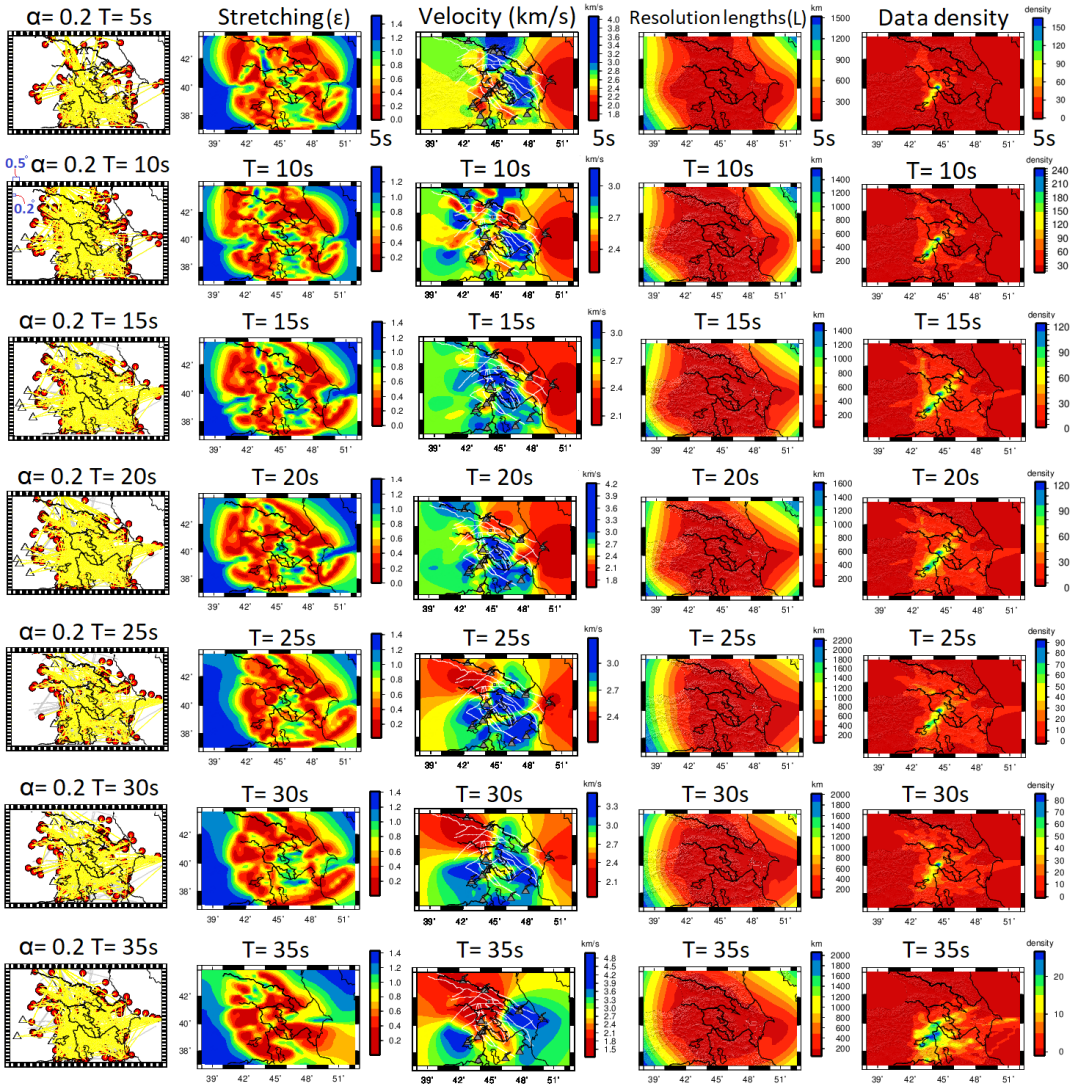

Figure 6: Variations in the 2D Rayleigh wave group velocity tomography maps and resolution parameters (averaging area (L), stretching value (ε), and data density) for short-periods (5, 10, 15, 20, 25 s), medium-periods (30, 35, 40, 45 s), and long-periods (50, 55, 60, 65, 70 s). The numbers 0.2° and 0.5° (at period 10 s) show the cell sizes used in this study. The white lines are faults, gray triangles are volcanoes and mountains, white triangles are seismic stations, and red circules show the epicenter of earthquakes. The yellow lines show the rays coverage between data and seismic stations. The gray lines show the inter-stations paths.

dle and van der Lee, 2009; *Porter et al.*, 2019] from within the Earth, the colors show anomalies in rigidity, which correlate with temperature anomalies. Hence, the dark blue-green-yellow shades mean colder and stiffer rock (fast regions) that are the remnants of an old tectonic plate that has been subducted underneath the Earth plates (large cold and aseismic area during million years) and dark red-orange shades mean warmer and weaker (slow regions).

The generated tomography velocity maps in this study (Figure 6) contain all of the above mentioned characteristics. Therefore, the commentary of these tomography maps based on the above specifications and comparison with the results of other tomography studies (different methods) performed in the region for velocity anomalies at different periods and depths is followed. Figure 5 shows the active tectonic features of the collision zone of the Central Eurasian-Arabian and geological units discussed in the interpretation of 2D tomography maps of the study area.

The minimum and maximum depth of our 2D tomography model is controlled by the wave velocity, shortest, and longest period of the observed dispersion curve, respectively. We did not consider periods longer than 70 s in the inversion procedure because of the low ray coverage for $T > 70$ s (Figure 4 g).

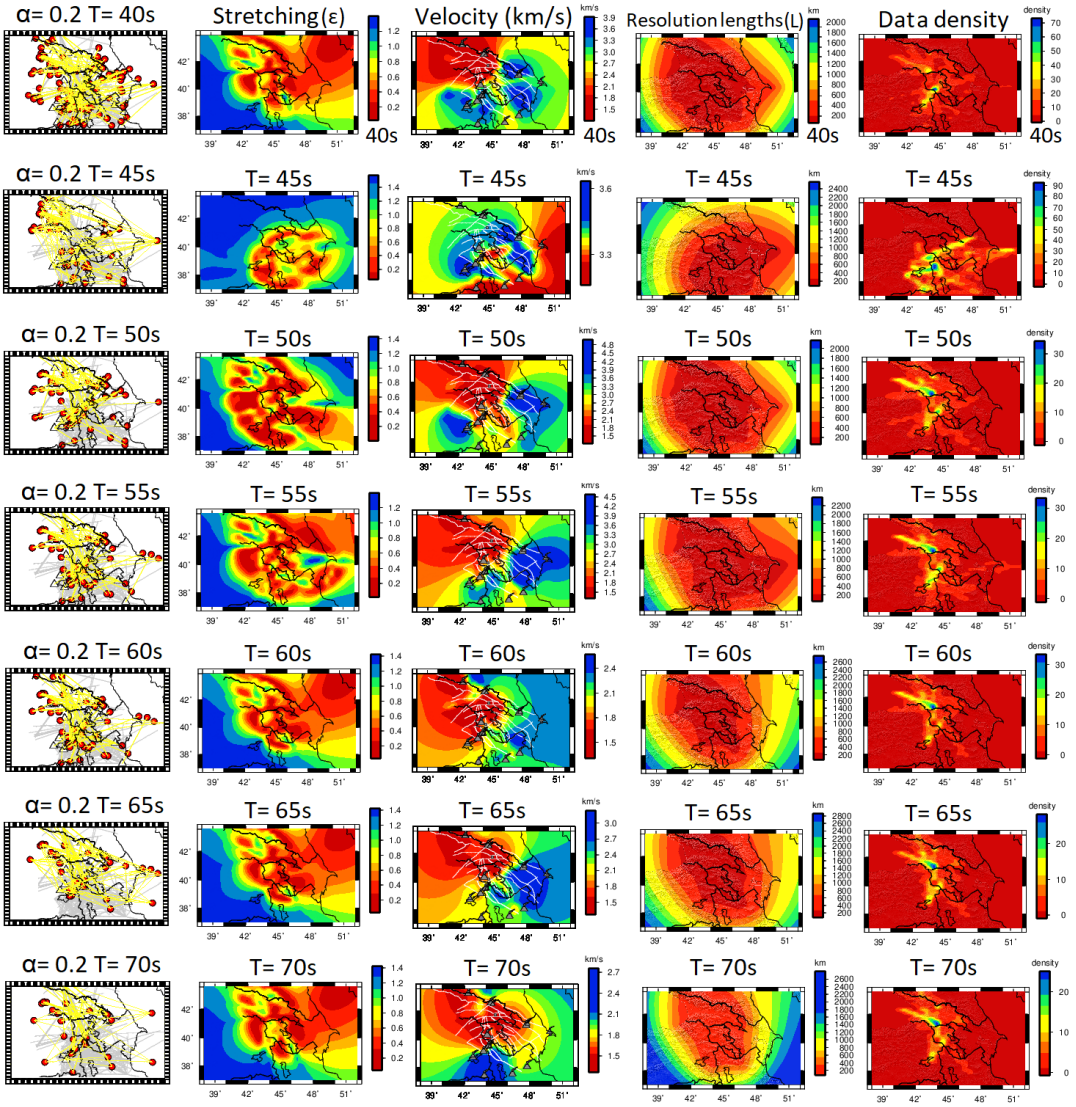

Figure 6: (continued).

As a rule of thumb, the maximum penetrating depth of the waves is defined by:

$$\text{Depth} = \frac{2}{3}\lambda = \frac{2}{3}\frac{V}{F},$$

and

$$F = \frac{1}{T} \Rightarrow \text{Depth} = \frac{2}{3}VT,$$

where λ is wavelength, V (velocity), F (frequency), and T (period). For example, from Figure 6 the range of group velocity for the period of 5 s is between 1.8 and 4 km/s, so the maximum depth will be in the range of 6 to 13.33 km.

Table A1 and A2 show quantitative information about the depth variations in different periods. As the sensitivity of depth was discussed in above, it is clear that the shallow structures (e.g., sedimentary basins such as SCB, KB, EBSB) are controled by the dispersion curves at short periods, while longer periods are more influenced by deeper structures.

For the short-periods of 5 to 25 s in our study (Figure 6), Rayleigh waves velocity are sensitive to the crust within a thickness less than 6 to 51.66 km, and they sample the whole crust with the maximum sensitivity at approximately 51.66 km. The velocity of Rayleigh waves at short periods, is containing information relative to shallow geological features, like sedimentary basins, topography (uplifts), and volcanic complexes. In the tomography maps of 5 and 10 s, we observe a relatively high-velocity anomaly along the southern Azerbaijan, TAL (Talesh), Sheki, BM, Tbilisi, Grozny (Terek basin), and Elbrus–Aragats–Kazbek volcanic complexes, which are confined by low-velocity anomalies in the SCB, KD, RB, Alazani, EBSB, EAAC, and eastern part of NTF.

We interpret that the low group velocities in the SCB, KB, RB, Alazani, and EBSB basins are related to the presence of thick sediments (~7 to 15 km; [*Jackson et al.*, 2002] and the low-velocity

zone beneath the volcanic complexes (e.g., Elbrus, Kazbek, Ararat, Aragats, Sahand) could be due to the high temperature of the volcanic rocks or shallow magma chamber beneath these volcanoes. In contrast, the high-velocity zones beneath the volcanoes could be due to low temperature volcanic rock or a deeper magma chamber.

In the Lesser Caucasus, there is the link between the volcanic manifestations and low-velocity patterns, but it is not as clear as in the Greater Caucasus. The Gegham volcanic group in Armenia also match with the location of the low-velocity anomaly, while one exception is for the Aragats volcano group in Armenia, which is situated with high-velocity feature (*however, our tomography map at period of 5 s, reveals a small low-velocity zone on the northwest slope of Aragats volcano at a depth of ~7 km, which is different from the results of other studies*). According to studies [e.g., *Koulakov et al.*, 2012; *Zabelina et al.*, 2016], this feature might be explained by the old age of this volcano which does not express any activity for more than half million years. This low-velocity is clearly consistent with the Kars volcanic group in northeastern Turkey and Javakheti (Dzhavakheti) in southern Georgia, which includes the Bakuiani, Samsary, and Dididuli mountains. In the LC, TAL, Elbrus, GC, and Kars altitudes, high- and low-velocity anomalies are seen at short ($T < 25$ s), medium ($T < 45$ s) and long ($T > 50$ s) periods, respectively, and they were interpreted as relative thickening of the crust.

For example, about the low-velocity beneath the volcanoes, [*Milyukov et al.*, 2018], showed the location of a magma chamber at depths of 1–8 km and extended magma source at depths of 15–40 km beneath the Elbrus eastern summit. The tomographic images of our study ($T = 10$ and 15 s) in the presence of the orange spots beneath the Elbrus and Ararat volcanoes with an approximate depth of 31 km (Figure 6) are consistent with the mentioned study of Milyukov.

Also, high-velocity anomalies observe beneath the volcanoes in the GC, LC, NW Iran, and EAAC ($T = 15$, 20, and 25 s) and extend over the study area; that may indicate a transition from warm magmatic rocks to cold ones. Meanwhile, along the BM, PT, GC, and LC low-velocity zones are observed, which can be related to the sedimentary and upper Paleozoic-Triassic metamorphic rocks in these supercomplexes [*Adamia et al.*, 2011].

On the obtained tomography maps in our study the broad low-velocity zone in the SCB, Baku–Kura, Central Armenia Block (CAB), and Sevan is observed. Some studies [e.g., *Abbasov*, 2016; *Bochud*, 2011] have identified the presence of hydrocarbon resources (several abundant major oil and gas fields) in the mentioned Troughs in Paleogene and Neogene strata. So, our obtained low-velocity maps could be a strong reason for this situation.

We infer that the comparison of surface velocity maps of the middle and lower crust [e.g., *Koulakov et al.*, 2012; *Zabelina et al.*, 2016], reveals this feature in the transition zone from SCB and KB to NW Iran, in which, the lower crust has high surface wave velocity (3.6 km/s) below Talesh, Transcaucasus Massif (TCM), and Kazbek (due to ongoing subduction or underthrusting of the Kura Basin lithosphere under the Scythian platform and existence of a stable and thick mantle). Contrarily, velocity decreases about 2.1 to 2.4 km/s below LC, EAAC, SCB, KB, Tabriz fault, Sahand, BM, and Yanardagh mountain (due to very thin lithosphere < 100 km or thin mantle coverage). In addition, the shallow Curie point depth observed by [*Aydın et al.*, 2005], which implies a shallow magma source, is well correlated with the observed our study low group velocities in the EAAC, Lake Van, and Lake Urmieh sedimentary basin.

Sun [2004], determined the depths of Moho (20–40 km) in Caucasus for different geological units. Also, in accordance with [*Fang*, 2010], the hot material of the uppermost mantle may migrate to the crust along the offset of Moho discontinuity, and intrusion of mantle material heats up the lower crust and can cause the reduction of seismic velocity. So, about the low-velocity anomalies at periods between 15 and 20 s ($\sim 26 <$ depth $\lesssim 42$ km – in our study), we conclude that the discontinuity of the Moho could be the strong reason (see section Appendix A, Figure A1).

The low-velocity regions (e.g., Ganja city, Mingachevir Damand, Sheki, Lake Van, Nakhchivan) that are located on a segment of Tabriz-Balykgel, Garni, PSS and Akerin faults, could be affected by fault thermal interactions. Also, the existence of basaltic eruptions in the Quaternary period, which confines it to late Pliocene folding, the tectonic activity of the faults, can be attributed to observed low-velocity anomalies inside the crust, as proposed by [*Keskin*, 2003].

In medium-periods (30 to 45 s), according to the penetrating depth of surface waves ($2\lambda/3$), the waves are primarily sensitive to depths between 68 to 108 km, and contains the velocity changes in the lower crust up to the uppermost mantle lid.

In most parts of NW Iran and LC (at $T = 15 - 35$ s), the velocities are approximately the same and show slight variation, which, indicates a laterally smooth velocity structure of the crust in these regions. In the SCB, Baku, and KB, the low-velocity anomaly is observed not only for short periods ($T = 5 - 25$ s) consistently with a thin or absent mantle lid, but also at medium-periods ($T = 30 - 45$ s). This indicates that the anomaly is not limited to the upper mantle, but it extends into

the lower crust where we observed lower velocities within the crust in the region of study. In this case, the main process of such intrusion, whose amount is reduced toward NW Iran, could be related to the existence of partial melting zones inside the crust [e.g., *Zabelina et al.*, 2016]. This condition in EAAC and located at the east and northeast of Lake Van shows probably the shallowest LAB (lithosphere-asthenosphere-boundary) depth in the study area. The high-velocity in the lower crust of SCB relative to NW Iran is probably because of the oceanic source of the lower crust in this region. High plateaus of EAAC and NW Iran are supported by hot asthenosphere with a wide spread uppermost mantle derived volcanism, and the very shallow LAB (~70 km) of EAAC region [e.g., *Skobeltsyn et al.*, 2014].

The prominent low-velocity area in the Southern Armenia Block on the Garni fault and the Zangezur Zone, could be evidence of interactions in the LAB or the LVZ (low-velocity-zone) discontinuities due to the sudden change in wave velocity from very high to low (5.04 to 2.52 km/s); [see section Appendix A, Figure A1]. In this case, seismic waves pass through the lithosphere-asthenosphere very slowly and wave velocity reduction from lithosphere to asthenosphere, could be caused by the presence of a very small percentage of melt in the asthenosphere. The upper mantle LVZ is a depth interval with slightly reduced seismic velocity compared to the surrounding depth intervals. The zone is present below a relatively constant depth of 100 km (in our study depth of 104 km, Figure A1) in most continental parts of the world [*Thybo*, 2006]. The LVZ, extends from about 65 to 220 km depth in the ocean basins [*Presnall and Gudfinnsson*, 2011].

About the low-velocity in NE Nakhchivan, based on study of [*Sosson et al.*, 2010], we interpret that due to the upper Devonian (the fourth period of the Paleozoic era) and Permian (the fifth period of the Paleozoic era) rocks, these rocks could be petroleum source rocks. Silurian and Lower and Middle Devonian marine clastic and carbonate rocks crop out in Nakhchivan and are presumed to be present in Armenia (Syunik highlands, Goris and Sisian cities).

Observed low-velocity in the western GC and high-velocity in the eastern GC could be in accordance with the interpretation of [*Ruppel and McNutt*, 1990], in which they suggested a weak, hot and thermally altered lithosphere under the western Greater Caucasus as opposed to a more elastic and cold lithosphere in the eastern Greater Caucasus.

The results for the long-periods (50–70 s – Figure 6) are different, and the north, northwest, and western areas (e.g., the western GC, LC, EAAC, EBSB, RB) show ultra-low group velocities, while the eastern and southern areas (e.g., the SCB, Azerbaijan, KB, TAL, NW Iran) show ultra-high group velocities. In this case (at a depth of ~180 km), the Rayleigh waves are mostly affected by the structure of the uppermost mantle velocity. We argue that lithospheric interactions generate low-velocity anomalies (due to thin lithosphere mantle, thin mantle cap) and high-velocity (mainly due to the stable continental mantle cap or an ocean-like cover).

For these deep areas lithospheric interactions is a mechanism of feeding the volcanoes due to the delaminated (missing) lithosphere detached due to collisional processes and overheated asthenosphere appears to be very close to the bottom of the crust and heats the crustal rocks, leads to active melting and forming magma reservoirs. Also, we infer that the occurrence of deep earthquakes (for example 2015-09-12 02:08:49, Latitude 43.67°N, Longitude 45.74°E, depth 121.66 m, M4, NEIC, eastern Caucasus in our study) could be a reason of thermal interactions beneath the Caucasus (east to west) due to active subduction (subducted, detached, and torn slabs) which presents a potentially larger seismic hazard than previously recognized and may explain historical records of large magnitude (~8) seismicity in this region [e.g., *Mumladze et al.*, 2015]. These commentaries are in good agreement with observed low-velocity anomalies at long-periods in Caucasus [e.g., *Koulakov et al.*, 2012].

A study of [*Mangino and Priestley*, 1998] indicates the high-velocity anomaly in the SCB that extends beneath Talesh, with a limited underthrusting of the SCB beneath Talesh which this result is in agreement with our high-velocity anomalies in the SCB and Talesh at long-periods (T = 50 to 70 s). Alternatively, this very high-velocity anomaly may be a lithospheric root that underlies the Kura Basin. However, as mentioned above, occurrence of deep earthquakes (100 to 250 km) in the north of the eastern Greater Caucasus are suggestive of ever-evolving subduction or underthrusting of the Kura Basin lithosphere beneath the eastern part of the Greater Caucasus [e.g., *Kovachev et al.*, 2009].

The pattern of the tomography velocity maps at periods of 50 to 70 s are similar and the whole Caucasus appears as a cratonic-like basement and the north-northwest of the Caucasus is covered by an ultra low-velocity anomaly, while the south-southeast areas are covered by an ultrahigh-velocity anomaly. At periods after 50 s (page 10), the group velocity map experiences lateral changes of 1.7 to 5.04 km/s and almost the entirety of the NW Iran, Armenia, Eastern Anatolia, and Georgia has been covered with a low-velocity anomaly.

These deep low-velocity zones follow the pattern described above for the LVZ and LAB discontinuities.

The existence of very deep low-velocity zone was initially alerted by seismologists and they gave some information about its physical properties, as the speed of seismic waves decreases with decreasing rigidity. Tomography maps at these depths (~160 km) show the effects of pasty and hot melt or perhaps magma chambers beneath the plateau area, and thus making possible volcanic activities in the future [e.g., *Condie*, 2001].

At the depths joint between the lithosphere-asthenosphere and the upper mantle; anomalies accumulation, inhomogeneities, onset of dry melting in the convecting mantle, and antagonistic behaviors (due to continuous changes in temperature of the plate tectonic activity and hot asthenospheric diapirs intrusion), the surface waves have variable behavior. Diagram of depth vs temperature of melting also shows that after depth of 100 km, the temperature has a significant upward trend and reaches to the 1400 °C at a depth of 150 km, which indicates that the upper mantle lid is covered with hot molten material [e.g., *Sugden et al.*, 2018].

At periods ranging from 50 to 70 s, NW Iran, GC, LC, and EAAC are dominated by a process of increasing temperature and a significant decrease in surface wave velocity. For these deep low-velocity anomalies, it appears the lithosphere-asthenosphere is hot beneath these areas. In contrast, for high-velocity regions; the upper mantle is thought to have been rejuvenated by a phase of upwelling mantle, and this metasomatic refertilization of the upper Cratonic mantle has increased its density and reduces seismic velocity [e.g., *Beccaluva et al.*, 2007]. Although because of the poor ray's coverage at long-periods, points obtained using tomography should be interpreted with caution.

4.1 Some useful lithospheric hints in accordance with previous studies in the enigmatic Caucasus

Our study 2D derived tomography maps reveals diverse velocity structures in the crust up to the uppermost mantle for the different geological units include GC, LC, RB, KB, NW Iran, SCB, EBCB, EAAC, TAL, BM, and several stratovolcano complex such as Elbrus, Kazbek, Aragats, Ararat, Sahand, and Sabalan to describe the regional tectonic activity in ever evolving zone of the Eurasian-Arabic plates, which these results are possibly associated with active tectonic processes occurring in the Caucasus region.

In accordance with results of some previous studies such as [e.g., *Koulakov et al.*, 2012] and others, the high-speed anomaly below the BM, PT, and NW Iran (depth > 120 km) could be the remnant segments of the the broken off chilled oceanic lithosphere or hot traces generated as the slabs were sinking into the mantle transition zone. Such large downward movements (e.g., EAAC) are free of extended lithospheric and indicates a very poor to absent mantle lid (thin lithosphere) for EAAC.

The structures with dark-red stains with depth up to ~ 20 km mostly demonstrate the alterations of deep sedimentary basins (e.g., SCB, EBSB, RB, Alazani, Aras, and KB) and basement of uplifted complexes (e.g., Elbrus, Kazbek). These prominent significant low-velocity anomalies, which are clearly expressed in our different periods of 2D tomography velocity maps, correspond to the velocity structure of the basins and volcanoes. The low-velocity spots (dark-red stains) beneath the volcanoes can also indicate a magma chamber.

The spread of high-velocity anomalies (dark blue) in some regions of the Greater Caucasus (east to west), northwest of Iran, BM and PT could be due to the thick lithosphere in these geological units with thicknesses ranging from 100 to 180 km. High-velocity anomalies after a depth of 130 km in the southeastern side of the Greater Caucasus (even SCB, Baku, northern part of the TAL region) to be very complicated in terms of tectonic activity due to continuous subduction. Also, the high-velocity anomalies indicate anomalous thickening of the crust during continental collisions, leading to sinking parts of the mantle lithosphere. The removal of the mantle part significantly reduces the lithosphere's strength and causes more shortening and mountain building and almost reaching to the ultra-hot (dark red) asthenosphere material.

Figure 7 shows the Caucasus 2D Rayleigh waves velocity tomography maps at periods 5 to 70 s with topographic coefficient (0.6) for comparing the anisotropic and distinct distribution of velocity anomaly in the geological units of the Caucasus with different short, medium, and long periods. The boundary between the surrounding mountain ranges and sediment basins is clearly outlined.

5 Discussion

The main goal of this study is investigating 2D tomography maps using surface wave dispersion in the Caucasus territory. Definitely, because of the source mislocation and error in the determination of the basic parameters of earthquakes such as the focal depth, latitude, longitude, and magnitude, dispersion measurements are not free of uncertainty. The prominent features of this study is that: first, the modified earthquake database that includes 19 years (1999–2018) was used and

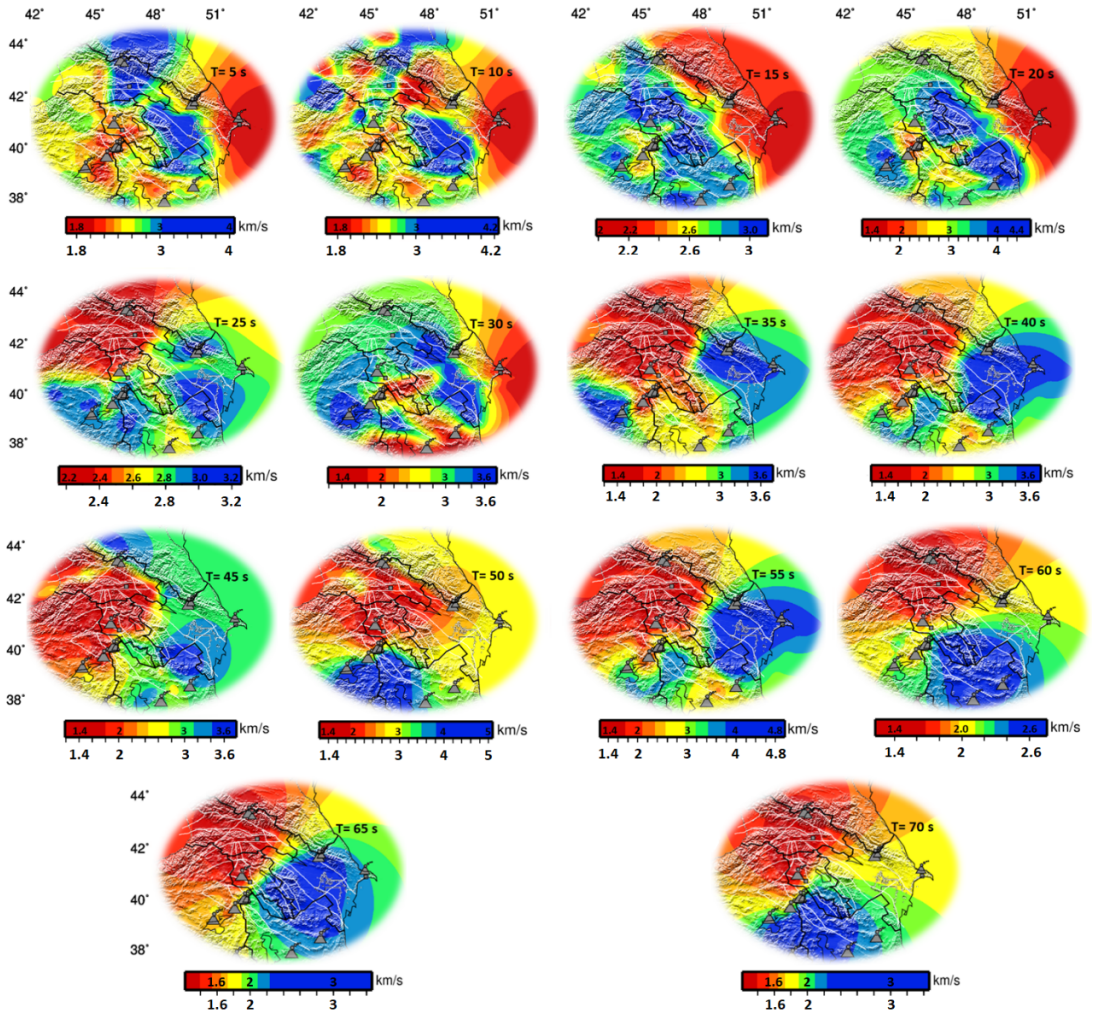

Figure 7: 2D Rayleigh velocity tomography maps for the Caucasus (periods of 5 to 70 s) with topographic coefficient 0.6 and ~ 30,000 processed vertical (Z) components of dispersion curve.

second, the study benefits from new seismic stations in northwest of Iran, Turkey, Georgia, Russia, Azerbaijan, and Armenia which creates a suitable coverage of the ray paths in the study area.

In this paper, the Caucasus 2D group velocity tomographic maps were successfully calculated using Rayleigh surface wave rays along with the resolution parameter maps, and those include the averaging area (L), stretching (ε), and data density across the Caucasus territory for an equivalent depth of ~ 180 km and at a period between 5 to 70 s. We described 2D tomography velocity maps variations in different major discontinuities, including Crust up to the Upper Mantle relying the increasing and decreasing the Rayleigh surface wave velocity and the results of previous studies in the study area.

Our study derived tomography maps reveal strongly various velocity structures (low and fast) for different geological units include GC, LC, RB, KB, NW Iran, SCB, EBCB, EAAC, TAL, BM, and several stratovolcano complexes such as Elbrus, Kazbek, Aragats, Ararat, Sahand, and Sabalan to more understand about the zonal tectonic activities in an ever-evolving deformations of the geological complexities of the Eurasia-Arabia plates.

As mentioned earlier, in comparison with previous tomographic studies with different methods, our results are consistent with the structures of geological units such as sediment basins, volcanic complexes, and uplifts in this region. The red shades (slow velocity) in our generated tomography maps for short-periods represent the alterations of deep-shallow sedimentary basins (e.g., SCB, EBSB, RB, Alazani, Aras, and KB) and uplifted basement complexes (e.g., GC, LC, and TAL). In this regard, from the perspective of our study tomography velocity maps (Figure 6), most volcanic complexes in the Caucasus (e.g., Elbrus, Kazbek, Sahand, and Sabalan) is correlated with low-speed anomalies.

Based on the results of other studies [e.g., *Koulakov et al.*, 2012] the expansion of high-velocity anomalies (dark blue-green shades) in

some parts across the Greater Caucasus (east to west), NW Iran, BM, and PT can be interpreted as thick plate lithosphere in these regions from 100 to 180 km. The observation of high-velocity anomalies after ~130 km depth in the southeast side of the Greater Caucasus (even SCB, Baku, north part of TAL area) show that due to continuous subduction, they tend to be very complicated in terms of the shape of tectonic activities. The basement of Transcaucasus (T = 10 and 30 s), which separates the Greater and Lesser Caucasus, is observed in the low-velocity anomaly zone, which may represent part of the interactions caused by the breaking of rocks of the Orkhoi, Gali, and Gagra faults.

The results of resolution length (averaging area – L) for most parts of the study area are about 50–150 km, but for marginal areas with low ray coverage, these values are even more. The stretching (ε) parameter values are spatial distribution (azimuthal coverage) of the paths, and large values of this parameter indicate the preferred orientation of the paths. The distribution of the stations and earthquakes controls the stretching (ε) parameter, which is beyond our control. Its smaller value (usually $\varepsilon < 1$) indicates a uniform distribution of rays and we obtained its value in our study about 0.7, which shows a uniform distribution and an identical resolution along each path for most parts of the study area (Figure 6 and Table A1).

6 Conclusions

To better understand the regional tectonic activities in the Caucasus, Rayleigh wave dispersion curves across the Caucasus are extracted from ~1300 earthquakes recorded at 49 permanent-temporary stations using the single-station method at a period of 5 up to 70 s. These high-resolution 2D tomography images give some new information about the complex velocity structures, tectonic interactions, and hot-cold lithospheric activities based on the wave velocity (slow and fast) changes at different period and depths in the ever-evolving collision zone of the Eurasian-Arabic plates. These maps show excellent agreement with many features of the geological units in the Caucasus.

The illustrated tomography maps of this study with different velocities for the short-medium periods ($5 \leq T \leq 45$ s; depth of ~ 6.66 to ~ 108 km) are more sensitive to structure of the upper crust up to the lower crust. These periods (T = 5 to 45 s) represent the activities and velocity structures in the sediment basins, molten material, magma chambers, and the uppermost part of the mantle lid.

The depicted tomography maps at long-periods ($50 \leq T \leq 70$ s; depth of ~ 180 km) are more influenced by the velocity structure of the uppermost mantle. Through investigation and comparison with the results of other studies in the Caucasus, it shows that the ultralow-velocity anomalies at these periods are mainly due to a thin lithosphere or due to the absence of lithospheric mantle. Contrarily, ultrahigh-velocities can be related to concentration of liquids in the compartment and the lack of hot asthenospheric diapirs.

Acknowledgements. Thanks to the Iranian Seismological Center, Incorporated Research Institutions for Seismology (IRIS) Data Management Centre, Iranian Seismological Center (IRSC), International Institute of Earthquake Engineering and Seismology (IIEES), Iranian National Seismological Network, and temporary network of the Institute for Advanced Studies in Basic Sciences (IASBS), who provided some of the seismic data used in this study. Our appreciation also goes to Prof. T. B. Yanovskaya for sharing her tomographic software, Wessel and Smith for GMT Tools, and the Institute of Geophysics of University of Tehran which managed and supported this study in the framework of the educational mission (2016–2018). Special thanks to Michael Smith (USA) & Natasha Lewis (USA) for editing the grammar of the article.

Appendix A

Table A1: Variations in the different parameters used in this study

Period (T) (Sec.)	Stretching value (ε)	Data density value	Averaging area (L) value (km)	Velocity (km/s)	Depth= $2VT/3$ (km)
5	0.6 <	160	~ 110	$1.8 \leq V \leq 4.0$	$6 \leq$ Dep. ≤ 13.33
10	0.6 <	240	~ 110	$2.0 \leq V \leq 4.2$	$13.33 \leq$ Dep. ≤ 26.66
15	0.5 <	160	~ 100	$2.0 \leq V \leq 3.0$	$20 \leq$ Dep. ≤ 30
20	0.55 <	120	~ 110	$2.5 \leq V \leq 4.4$	$33.33 \leq$ Dep. ≤ 58.66
25	0.6 <	80	~ 90	$2.4 \leq V \leq 3.0$	$40 \leq$ Dep. ≤ 50
30	0.5 <	80	~ 150	$2.2 \leq V \leq 3.4$	$44 \leq$ Dep. ≤ 68
35	< 0.5	~25	~ 180	$2.6 \leq V \leq 3.6$	$60.66 \leq$ Dep. ≤ 84
40	~ 0.5	70	~ 200	$1.6 \leq V \leq 3.6$	$42.66 \leq$ Dep. ≤ 96
45	0.7 <	8	~ 250	$3.2 \leq V \leq 3.6$	$96 \leq$ Dep. ≤ 108
50	~ 0.85	~ 30	~ 250	$1.7 \leq V \leq 5.04$	$56.66 \leq$ Dep. ≤ 168
55	0.90 <	~ 30	~ 220	$1.6 \leq V \leq 4.76$	$58.66 \leq$ Dep. ≤ 174.53
60	0.86 <	~ 30	~ 220	$1.5 \leq V \leq 2.52$	$60 \leq$ Dep. ≤ 100.8
65	0.8 <	~ 23	~ 280	$1.5 \leq V \leq 3.36$	$65 \leq$ Dep. ≤ 145.6
70	0.8 <	~ 23	~ 290	$1.4 \leq V \leq 3.37$	$65.33 \leq$ Dep. ≤ 157.26

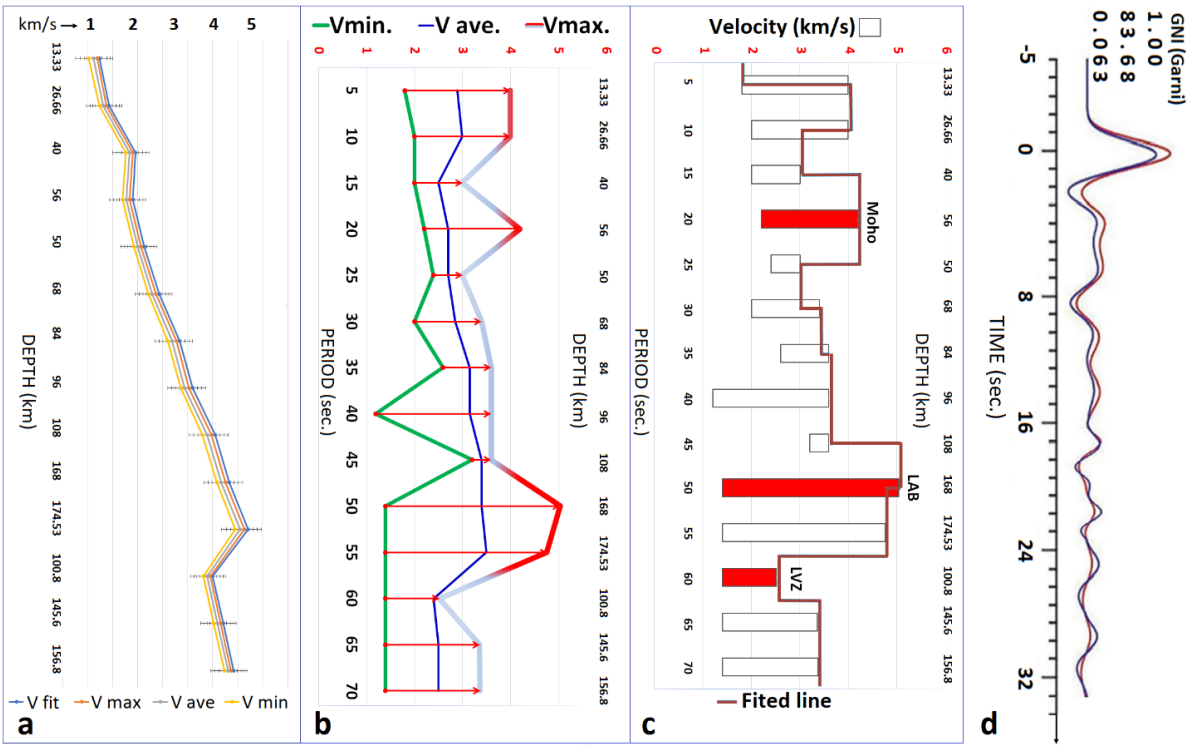

Figure A1: In the calculations of this study, the drawing of kernel curves and velocity models for different geological units or tectonic zones in the Caucasus territory (such as LC, GC, northwestern Iran, EAAC, etc.) due to the workload of data processing was avoided. In contrast, velocity-depth-period curves, in order to estimate the approximate position of the Moho, LAB, and LVZ discontinuities using increasing and decreasing wave velocity versus depth-period (only to describe 2D tomographic maps obtained at long-medium periods) were plotted. For this purpose, specialized computer codes in MATLAB software, Stock Method, and Riemann Sum were used. Figs. a) and b) show the diagram of velocity changes vs. depth-period. c) Velocity model corresponding to the possible LAB, Moho, and LVZ relative to the group velocity. d) A sample of receiver function signal (observational – blue and predicted – brown-red).

Table A2: Variations in velocity, period, and depth parameters

Period (sec)	P5	P10	P15	P20	P25	P 30	P 35	P 40	P45	P 50	P 55	P60	P 65	P 70
Period (sec)	5	10	15	20	25	30	35	40	45	50	55	60	65	70
Depth (km)	13.33	28	31	58.66	53.33	68	73.5	96	102	168	174.16	104	147.33	158.66
V Max. (km/s)	4	4.2	3.1	4.4	3.2	3.4	3.6	3.6	3.6	5.04	4.75	2.6	3.4	3.4
V Ave. (km/s)	2.9	2.1	2.7	3.25	2.75	2.85	3.15	3.15	3.4	3.39	3.12	2.1	2.45	2.35
V Min. (km/s)	1.8	2.1	2.3	2.1	2.3	2.3	2.7	1.7	3.2	1.75	1.5	1.6	1.5	1.3

References

Abbasov, O. R. (2016), Geological and geochemical properties of oil shale in Azerbaijan and petroleum potential of deep-seated Eocene-Miocene deposits, *European Journal of Natural History*, (2), 31–40.

Adamia, S., G. Zakariadze, T. Chkhotua, N. Sadradze, N. Tsereteli, A. Chabukiani, and A. Gventsadze (2011), Geology of the Caucasus: A Review, *Turkish Journal of Earth Sciences*, *20*(5), 489–544,, doi:10.3906/yer-1005-11.

Ammon, C. J. (2019), Seismic Waves and Earth's Interior, http://eqseis.geosc.psu.edu/cammon/HTML/Classes/IntroQuakes/Notes/waves_and_interior.html.

Aydın, İ., H. İ. Karat, and A. Koçak (2005), Curie-point depth map of Turkey, *Geophysical Journal International*, *162*(2), 633–640, doi:10.1111/j.1365-246X.2005.02617.x.

Beccaluva, L., A. Azzouni-Sekkal, A. Benhallou, G. Bianchini, R. Ellam, M. Marzola, F. Siena, and F. Stuart (2007), Intracratonic asthenosphere upwelling and lithosphere rejuvenation beneath the Hoggar swell (Algeria): Evidence from HIMU metasomatised lherzolite mantle xenoliths, doi:10.1016/j.epsl.2007.05.047.

Bedle, H., and S. van der Lee (2009), *S* velocity variations beneath North America, *Journal of Geophysical Research: Solid Earth*, *114*(B7), B07,308, doi:10.1029/2008JB005949.

Bochud, M. (2011), Tectonics of the Eastern Greater Caucasus in Azerbaijan, Ph.D. thesis, University of Fribourg.

Condie, K. C. (2001), *Mantle Plumes and their Record in Earth History*, Cambridge University Press, doi:10.1017/cbo9780511810589.

DeMets, C., R. G. Gordon, D. F. Argus, and S. Stein (1990), Current Plate Motions, *Geophysical Journal International*, *101*(2), 425–478, doi:10.1111/j.1365-246x.1990.tb06579.x.

Ditmar, P. G., and T. Yanovskaya (1987), A generalization of the Backus-Gilbert method for estimation of lateral variations of surface wave velocity, *Izv. Phys. Solid Earth*, *23*, 470–477.

Fang, L. (2010), Rayleigh wave tomography in North-China from ambient seismic noise, Ph.D. thesis, Universitá degli studi di Trieste.

Golonka, J. (2004), Plate tectonic evolution of the southern margin of Eurasia in the Mesozoic and Cenozoic, in *EUROPROBE, GeoRift 3: Intraplate Tectonics and Basin Dynamics. The Lithosphere of the Southern Eastern European Craton and its Margin*, vol. 381, pp. 235–273, doi:10.1016/j.tecto.2002.06.004.

Herrmann, R. B. (2013), Computer Programs in Seismology: An Evolving Tool for Instruction and Research, *Seismological Research Letters*, *84*(6), 1081–1088, doi:10.1785/0220110096.

Herrmann, R. B., and C. J. Ammon (2004), Computer programs in seismology. 3.30[cp/ol], http://www.eas.slu.edu/eqc/eqccps.html.

Ismail-Zadeh, A., S. Adamia, A. Chabukiani, T. Chelidze, S. Cloetingh, M. Floyd, A. Gorshkov, A. Gvishiani, T. Ismail-Zadeh, M. K. Kaban, F. Kadirov, J. Karapetyan, T. Kangarli, J. Kiria, I. Koulakov, J. Mosar, T. Mumladze, B. Müller, N. Sadradze, R. Safarov, F. Schilling, and A. Soloviev (2020), Geodynamics, seismicity, and seismic hazards of the Caucasus, *Earth-Science Reviews*, *207*, 103,222, doi:10.1016/j.earscirev.2020.103222.

Jackson, J., K. Priestley, M. Allen, and M. Berberian (2002), Active tectonics of the South Caspian Basin, *Geophysical Journal International*, *148*(2), 214–245, doi:10.1046/j.1365-246X.2002.01588.x.

Jin, D. J., and R. J. Colby (1991), A basic program to compute seismic surface-wave group-velocity dispersion curves, *Computers & Geosciences*, *17*(6), 777–799, doi:10.1016/0098-3004(91)90060-q.

Jrbashyan, R., G. Chlingaryan, Y. Kagramanov, A. Karapetyan, M. Satian, Y. Sayadyan, and H. Mkrtchyan (2001), Geology of Meso-Cenozoic Basins in Central Armenia, with Comment on Indications of Hydrocarbons, *Search and Discovery*, (30007).

Keskin, M. (2003), Magma generation by slab steepening and breakoff beneath a subduction-accretion complex: An alternative model for collision-related volcanism in Eastern Anatolia, Turkey, *Geophysical Research Letters*, *30*(24), doi:10.1029/2003GL018019.

Khuduzade, A. I., and A. Jafarov (2017), Structural-tectonic features of the south-eastern part of the Greater Caucasus the pre-Caspian GUBA as an example of the NQR, *Seismoprognosis observations in the territory of Azerbaijan*, *14*(1), 42–46.

Koulakov, I., I. Zabelina, I. Amanatashvili, and V. Meskhia (2012), Nature of orogenesis and volcanism in the caucasus region based on results of

regional tomography, *Solid Earth*, *3*(2), 327–337, doi:10.5194/se-3-327-2012.

Kovachev, S. A., V. G. Kaz'min, I. P. Kuzin, and L. I. Lobkovsky (2009), New data on mantle seismicity of the caspian region and their geological interpretation, *Geotectonics*, *43*(3), 208–220, doi:10.1134/s0016852109030030.

Mangino, S., and K. Priestley (1998), The crustal structure of the southern Caspian region, *Geophysical Journal International*, *133*(3), 630–648, doi:10.1046/j.1365-246x.1998.00520.x.

Milyukov, V., E. Rogozhin, A. Gorbatikov, A. Mironov, A. Myasnikov, and M. Stepanova (2018), Contemporary State of the Elbrus Volcanic Center (The Northern Caucasus), *Pure and Applied Geophysics*, *175*(5), 1889–1907, doi:10.1007/s00024-017-1595-x.

Mumladze, T., A. M. Forte, E. S. Cowgill, C. C. Trexler, N. A. Niemi, M. B. Yıkılmaz, and L. H. Kellogg (2015), Subducted, detached, and torn slabs beneath the greater caucasus, *GeoResJ*, *5*, 36–46, doi:10.1016/j.grj.2014.09.004.

Porter, R. C., S. van der Lee, and S. J. Whitmeyer (2019), Synthesizing EarthScope data to constrain the thermal evolution of the continental u.s. lithosphere, *Geosphere*, *15*(6), 1722–1737, doi:10.1130/ges02000.1.

Presnall, D. C., and G. H. Gudfinnsson (2011), Oceanic Volcanism from the Low-velocity Zone – without Mantle Plumes, *Journal of Petrology*, *52*(7–8), 1533–1546, doi:10.1093/petrology/egq093.

Rahimi, H., F. F. Mahdavyan, H. Zandi, and N. M. Beygi (2014), Velocity structure in North part of Iranian Plateau, in *Proceedings of the 16th Conference of Geophysics in Iran, 13–15 May, Tehran, Iran*, University of Tehran.

Ruppel, C., and M. McNutt (1990), Regional compensation of the Greater Caucasus mountains based on an analysis of Bouguer gravity data, *Earth and Planetary Science Letters*, *98*(3), 360–379, doi:10.1016/0012-821x(90)90037-x.

Skobeltsyn, G., R. Mellors, R. Gök, N. Türkelli, G. Yetirmishli, and E. Sandvol (2014), Upper mantle *S* wave velocity structure of the East Anatolian-Caucasus region, *Tectonics*, *33*(3), 207–221, doi:10.1002/2013tc003334.

Sosson, M., N. Kaymakci, R. Stephenson, F. Bergerat, and V. Starostenko (2010), Sedimentary basin tectonics from the black sea and caucasus to the arabian platform: introduction, *Geological Society, London, Special Publications*, *340*(1), 1–10, doi:10.1144/sp340.1.

Sosson, M., R. Stephenson, and S. Adamia (2017), Tectonic Evolution of the Eastern Black Sea and Caucasus: an introduction, *Geological Society, London, Special Publications*, *428*(1), 1–9, doi:10.1144/sp428.16.

Sugden, P. J., I. P. Savov, M. Wilson, K. Meliksetian, G. Navasardyan, and R. Halama (2018), The Thickness of the Mantle Lithosphere and Collision-Related Volcanism in the Lesser Caucasus, *Journal of Petrology*, *60*(2), 199–230, doi:10.1093/petrology/egy111.

Sun, Y. (2004), Adaptive Moving Window Method for 3D P-Velocity Tomography and Its Application in China, *Bulletin of the Seismological Society of America*, *94*(2), 740–746, doi:10.1785/0120030129.

Sun, Y., M. N. Toksöz, R. J. Martin, M. Krasovec, D. Yu, Q. Liu, and J. Liu (2012), Crustal and uppermost mantle structure of Caucasus and surrounding regions, *Earthquake Science*, *25*(5–6), 505–515, doi:10.1007/s11589-012-0874-y.

Thybo, H. (2006), The heterogeneous upper mantle low velocity zone, *Tectonophysics*, *416*(1–4), 53–79, doi:10.1016/j.tecto.2005.11.021.

Yanovskaya, T. B. (1997), Resolution estimation in the problems of seismic ray tomography, *Izv. Phys. Solid Earth*, *33*(9), 762–765.

Yanovskaya, T. B., and P. G. Ditmar (1990), Smoothness criteria in surface wave tomography, *Geophysical Journal International*, *102*(1), 63–72, doi:10.1111/j.1365-246x.1990.tb00530.x.

Yanovskaya, T. B., E. S. Kizima, and L. M. Antonova (1998), Structure of the crust in the Black Sea and adjoining regions from surface wave data, *Journal of Seismology*, *2*(4), 303–316, doi:10.1023/a:1009716017960.

Zabelina, I., I. Koulakov, I. Amanatashvili, S. E. Khrepy, and N. Al-Arifi (2016), Seismic structure of the crust and uppermost mantle beneath Caucasus based on regional earthquake tomography, *Journal of Asian Earth Sciences*, *119*, 87–99, doi:10.1016/j.jseaes.2016.01.010.